Parametric study and optimization on exhaled particle dispersion in a ward heated by impinging jet ventilation using orthogonal-based grey relational method

Parametric study and optimization on exhaled particle dispersion in a ward heated by impinging jet ventilation using orthogonal-based grey relational method

Teng Li[1], Jiangang Lei[1], Hanwen Luo[1], Emmanuel A. Essah[2], Yong Cheng[1,3,4*]

[1]School of Civil Engineering, Chongqing University, Chongqing, China

[2]School of Construction Management and Engineering, The University of Reading, United Kingdom

[3]Joint International Research Laboratory of Green Buildings and Built Environments, Ministry of Education, Chongqing University, Chongqing, China

[4]National Centre for International Research of Low-carbon and Green Buildings, Ministry of Science & Technology, Chongqing University, Chongqing, China

*Corresponding author. Tel.: +86 2365123213; E-mail: yongcheng6@cqu.edu.cn

Abstract

During the heating season with high-frequency infection events, an appropriate ventilation method is critical to a healthy hospital environment. In this study, impinging jet ventilation (IJV) was proposed to reduce cross-infection risk in a two-bed ward for winter heating. An Eulerian-Lagrangian approach validated by experimental data was employed to simulate exhaled particle dispersion. Using a full factorial design method, under air changes per hour (ACH) of 6 – 15 h^{-1} and supply air temperature (T_s) of 24 – 30°C, the effects of supply air parameters on particle dispersion was analyzed. A correlation model was subsequently established to delineate the relationship between supply air parameters and particle elimination. With an orthogonal-based grey relational method, this study compared the contribution and significance of supply air parameters and two uncontrollable factors (i.e., source location and outdoor air temperature), and then optimized the supply air parameters of IJV. The results indicated that the contribution percentage of supply air parameters was higher than 70% for particle removal and residence time. With an appropriate supply air parameter, the airflow of IJV could comply with human body plume, enhancing removal of fine particles (≤ 20 μm). However, with a low T_s (lower than 26°C) or an excessive ACH (more than 12 h^{-1}), the number of fine particles moving upwards

might be reduced. To achieve a better performance in preventing cross-infection, ACH and T_s of IJV were recommended to be set at 9 h^{-1} and 28°C, respectively. The findings were expected to provide guidance for ward ventilation design.

Keywords: impinging jet ventilation, supply air parameter, heating, hospital ward, optimization

Nomenclature

Ar	Archimedes number	x_i	reference value
C_D	drag coeffcient	y_i	predicted value
Δ_{max}	the maximum value in the deviation sequence	y^+	average non-dimensional distance of walls
Δ_{min}	the minimum value in the deviation sequence	$\eta_{D,fp}$	average deposition fraction of fine particles
d_p	particle diameter (m)	$\eta_{R,fp}$	average removal fraction of fine particles
ε	turbulent kinetic energy dissipation rate (m^2/s^3)	$\eta_{deposition}$	particle deposition fraction
F_a	additional forces exerted on the particle (m/s^2)	$\eta_{removal}$	particle removal fraction
F_i	external forces exerted on the particle in i direction (m/s^2)	$\eta_{suspension}$	particle suspension fraction
g	gravitational acceleration (m/s^2)	$n_{deposition}$	the number of particles deposited on solid surfaces
IL	infector location	$n_{removal}$	the number of particles removed by exhaust air outlet
K	heat transfer coefficient ($W/(m^2 \cdot K)$)	$n_{suspension}$	the number of particles suspended in indoor air
k	turbulent kinetic energy (m^2/s^2)	n_{total}	total number of particles exhaled by infector
k_{ij}	mean value of the response indicator	φ	normal distribution random number
$k_{ij,max}$	the maximum mean value of the response indicator	ϕ	physical parameter
$k_{ij,min}$	the minimum mean value of the response indicator	Γ	effective diffusion coefficient
l	total number of levels for Factor i	ξ	distinguishing coefficient

n	the number of reference points	$\xi_{0,i}(j)$	grey correlation coefficient
Re	Reynolds number		***Abbreviations***
R_i	range value of Factor i	ACH	air changes per hour
ρ	the density of air (kg/m^3)	ANOVA	analysis of variance
ρ_p	the density of particle (kg/m^3)	CFD	computational fluid dynamics
S	source term	COVID-19	coronavirus disease 2019
τ	average particle residence time	DeV	deflection ventilation
T_{out}	outdoor air temperature	DO	discrete coordinate
T_s	supply air temperature	DPM	discrete phase model
μ	the molecular viscosity of air (kg/(m·s))	DRW	discrete random walk
v_i	velocity component in i direction (m/s)	DV	displacement ventilation
v_{pi}	velocity component of particle in i direction (m/s)	GRG	grey relational grade
$\bar{v}$	time-averaged air velocity (m/s)	IJV	impinging jet ventilation
v'	the fluctuating component of air velocity (m/s)	MAE	mean absolute error
X_0	reference sequence	MV	mixing ventilation
$x_i(j)$	normalized value of the response indicator	RNG	renormalization group
x_{ij}	response indicator value	SIMPLE	semi-implicit method for pressure linked equation
$max\{x_{ij}\}$	the maximum value of the response indicator	SV	stratum ventilation
$min\{x_{ij}\}$	the minimum value of the response indicator	WAV	wall attachment ventilation

1. Introduction

Medical buildings are characterized by high source intensity, large population density, long occupation time and low occupant immunity, with a high probability of cross-infection [1-3]. Recently, with the global pandemic of coronavirus disease 2019 (COVID-19) and influenza, hospitals were facing greater threats. Under the influence of high virus activity [4-6] and decreased immunity of occupants, the number of people diagnosed with respiratory diseases in winter was more than that in summer. There was further evidence to demonstrate that the transmission of infectious diseases, including COVID-19, was associated with ventilation and indoor air movement [7-10]. Therefore, it was emphasized the

importance of an appropriate ventilation method for hospital wards and suitable parameters for air supply in winter.

Mixing ventilation (MV) was the most common ventilation method in hospital wards, which diluted contaminants by mixing the supplied clean air with indoor air [11, 12]. In the room served by MV, the conditioned air entered into the occupied zone through the supply air inlet located on the ceiling. In heating mode, a positive air temperature gradient could be found in the room and the thermal stratification might deteriorate its heating performance [13-15]. Displacement ventilation (DV) could create a stratified flow in cooling mode. The air lake at the bottom of the room could provide occupants with quality inhaled air [16, 17]. However, the heating application of DV was unsuitable due to the fact that low momentum supplied air of DV was difficult to penetrate into the occupied zone under the influence of thermal buoyancy [18].

Some advanced ventilation methods, such as stratum ventilation (SV), wall attached ventilation (WAV) and deflection ventilation (DeV), could exhibit better performance for indoor air quality in winter. SV supplied the air through the inlet located slightly above the head level of occupants [19]. In this way, the distance between the supply air inlet and the occupied zone was shortened and the warm air from the inlet could be effectively transported [20, 21]. Compared to traditional MV, SV could reduce the exhaled particle concentration at the breathing zone during winter [13]. The simulation results showed that in heating mode, SV improved inhaled air quality, with air change efficiency higher than 1.5 at the breathing zone [20]. For WAV, warm air was supplied downwards through an inlet located on the ceiling. The air inlet for WAV was close to the wall, so supply air jet could be attached to the surface of the wall due to the Coanda effect [22]. Simulation results showed that the average CO_2 concentration was around 470 ppm in the breathing zone under WAV [23]. Compared to MV, WAV provided a lower mean age of air and a higher contaminant removal efficiency for winter heating [24]. For DeV, a deflector was installed on the wall. The downward supplied air could be transferred directly to the occupied zone after collision with the deflector [25]. A case study showed that DeV could provide more fresh air and heat to the occupied zone in winter compared with traditional MV [26].

Impinging jet ventilation (IJV), an advanced downward ventilation method, supplied the air from the

duct located on the side wall [27]. The air jet of IJV impinged onto the floor and penetrated into the occupied zone along the floor. IJV combined the advantages of MV and DV and had potential to improve thermal comfort, air quality and energy efficiency. In some previous studies, this ventilation method had demonstrated its good ventilation performance and had been applied to cool different buildings. A case study showed that the classroom ventilated by IJV had a higher ventilation efficiency and a wider range of fresh air lake compared with DV in cooling mode [27]. In an office-layout room, Chen et al. [28] investigated the interaction between the cool supply airflow of IJV and the plume from heat source. The results of Su et al. [29] showed that the infection probability of nine susceptible persons under IJV was less than 1.5%. In order to improve indoor air quality and energy efficiency of IJV, Hu et al. [30] investigated its thermal stratification in summer. In a densely occupied classroom, Qin et al. [31] investigated the effect of exhaust location on the removal of exhaled contaminants under IJV. In large industrial premises, the results showed IJV created a satisfactory indoor environment and provided better working safety [32]. In cooling mode, the wide air lake formed along the floor under IJV, which could provide occupants with high-quality inhaled air [27, 32]. Additionally, IJV could be applied for winter heating [16]. The supply air jet of IJV had high momentum, which enabled the supplied warm air to overcome the buoyancy force and enter into the occupied zone [16]. Ye et al. [33] found significant difference in the airflow patterns of IJV between heating and cooling modes, and they quantified the warm air spreading distance of IJV. Staveckis and Borodinecs [34] studied the ventilation performance of IJV in an office room in winter. They found that the shape of inlet had a small effect on contaminant removal effectiveness. Yamasawa et al. [35] measured the contaminant distribution in an office-layout field chamber heated by IJV. They pointed out that the appropriate supply air parameters of IJV could achieve a contaminant removal efficiency higher than unity. Ameen et al. [36, 37] found that IJV performed better than traditional MV system in terms of indoor air quality in heating mode. Ye et al. [38] conducted simulations to compare the contaminant distributions in large-height spaces between IJV and MV in heating mode. The results showed that IJV could remove more gaseous pollutant and fine particles. These studies showed that IJV could achieve effective air delivery with a high contaminant removal efficiency, showing that IJV has potential to reduce the infection risk of people in hospital wards.

Since these previous studies are based on the non-healthcare buildings, there are significant differences

in the requirement for supply air parameter, the characteristics of heat and pollution sources and indoor furniture layout compared to hospital wards [7]. Therefore, the related results based on the non-healthcare buildings might not be suitable to hospital wards. Recently, Wang et al. [39] had confirmed that in summer, IJV could be used as an effective cross-infection control measure in intensive care unit ward. In another study, they investigated the thermal stratification of IJV and its effect on contaminant distribution in cooling mode [40]. However, a large number of medical devices with high heat generation are located in intensive care unit wards, and there are distinct differences in indoor air distribution and exhaled particle dispersion characteristic between the intensive care unit ward and general hospital ward. Additionally, due to the opposite direction of thermal buoyancy force, the airflow pattern of IJV in winter can be distinct from that in summer [33]. The results based on cooling mode cannot be applied directly in heating mode. Seasonal outbreak of respiratory disease emphasized the importance of work on ventilation and indoor air quality during winter.

In order to create a healthy hospital environment, IJV with high contaminant removal potential was proposed to reduce cross-infection risk in hospital wards for winter heating. This study aimed to investigate the exhaled particle dispersion characteristics in the ward heated by IJV and the effects of supply air parameters on particle dispersion. Using computational fluid dynamics (CFD) method based on Eulerian-Lagrangian approach, this study calculated the particle concentration, particle fate, particle residence time and trajectory under different supply air parameters. Based on the full factorial design method, the effects of supply air parameters on particle movement were revealed. Considering the effects of infector location and outdoor air temperature, an orthogonal-based grey relational method was then used to obtain the optimal supply air parameters. The results derived from this study could assist in providing the appropriate ward ventilation design and operation regulation strategy.

2. Methodology

2.1 Description of the geometry

The establishment of geometric model and the separation of computational domain were achieved by ICEM, a component in the ANSYS software. The two-bed hospital ward had dimensions of 4200 mm in length (X), 3600 mm in width (Y), and 2800 mm in height (Z), as shown in Fig. 1. Except for the

exterior wall and window on the left side of the ward, other walls were internal. The exterior wall contained a window with the area of around 4.0 m^2 (2860 mm × 1400 mm). Inside the ward, two patients were lying on their beds and a health care worker was standing on the floor. Three thermal manikins were simplified by rectangular block groups with the similar height and surface area to a normal adult since this study focused on the effect of global airflow pattern on exhaled particle dispersion [26]. The warm air was supplied downwards from the duct installed on the back wall. To alleviate particle resuspension, the installation height of inlet was 1000 mm above the floor [41]. The dimensions of inlet were 250 mm × 250 mm. To enhance the extract effect of thermal plume, the exhaust air outlet of IJV was located on the ceiling, with dimensions of 300 mm × 300 mm [42].

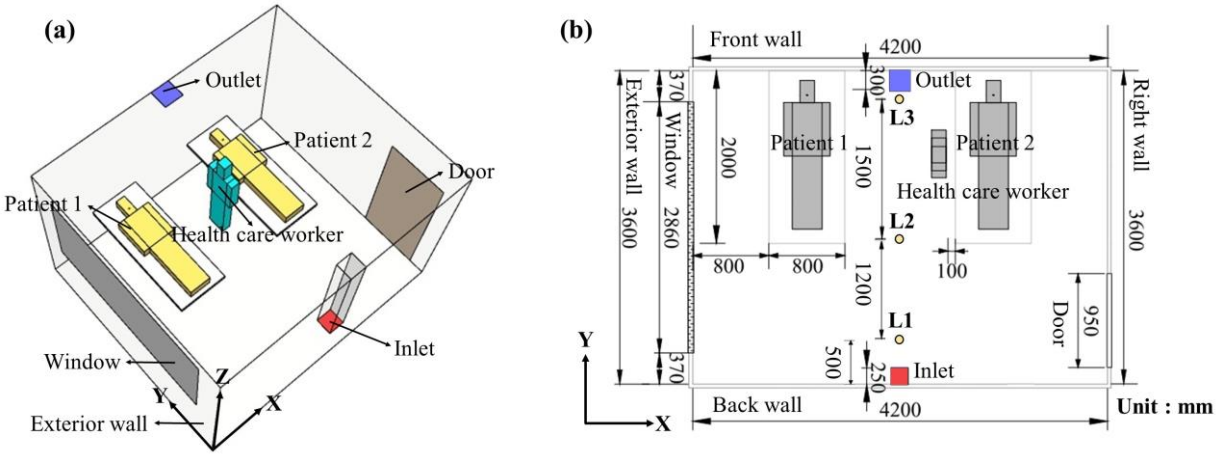

Fig. 1 (a) 3D schematic of studied ward, (b) Schematic plan of studied ward.

2.2 Numerical method

An Eulerian-Lagrangian approach was used for numerical calculation in FLUENT software. The renormalization group (RNG) *k-ε* model and the discrete phase model (DPM) were used to simulate the airflow field and particle dispersion [43], respectively.

2.2.1 Airflow phase

Table 1 lists the boundary conditions for airflow phase. In all cases, the inlet was set as velocity-inlet and provided full fresh air. The outflow condition was defined for the exhaust outlet. The health care worker and each patient generated the heat of 70 W and 80 W, respectively [44]. The heat transfer difference on a surface at different heights were ignored, and all walls were set as uniform heat flux.

Based on Chinese National Standard GB 50189-2015 [45], the heat transfer coefficients (K) of the exterior wall and window were set as 1.0 W/(m^2·K) and 3.0 W/(m^2·K), respectively. The right wall and door opposite the exterior enclosures were adjacent to a corridor without air-conditioning services, with the K values of 1.3 W/(m^2·K) and 1.6 W/(m^2·K), respectively. The air temperature in the corridor was assumed to be 5°C higher than outdoor air temperature [46]. Other surfaces (ceiling, floor, bed and interior walls) were considered to be adiabatic.

$$div(\rho v_i \phi) = div(\Gamma grad\phi) + S \quad (1)$$

Where ρ is air density (kg/m^3), v_i is the velocity component in i direction (m/s), ϕ represents the physical parameter, Γ is effective diffusion coefficient, and S is source term.

Considering computational accuracy and cost, the RNG k-ε model was selected to model turbulence [47]. The general governing equation for steady flow was given by Eq. (1). The finite volume method was used to convert the governing equations into algebraic equations. The convection and diffusion equations were discretized by second-order upwind schemes. The airflow field was calculated by the semi-implicit method for pressure linked equations (SIMPLE) algorithm. The effect on buoyancy force caused by varied air density was considered by Boussinesq hypothesis. Discrete coordinate (DO) model was used to calculate the radiation heat transfer. All solid surfaces inside the ward were defined as no-slip walls. The average non-dimensional distance of walls (y^+) was less than 5. The enhanced wall treatment was enabled to improve the calculation accuracy in near-wall regions. The convergence of the solution was monitored by residuals. The convergence criterion was set at 10^{-6} for energy and 10^{-4} for other variables.

Table 1 Boundary conditions for numerical simulation.

Type	Boundary condition	Discrete phase boundary condition
Inlet	Velocity-inlet	Escape
Mouth	Velocity-inlet	Surface injection Initial velocity, 0.5 m/s Initial temperature, 35°C Density, 1026 kg/m^3 Diameter, 0.5, 1, 5, 10, 20, 30, 40, 50, 75 and 100 μm

Outlet	Outflow	Escape
Exterior wall	Constant heat flux, K = 1.0 W/(m^2·K)	Trap
Exterior window	Constant heat flux, K = 3.0 W/(m^2·K)	Trap
Right wall	Constant heat flux, K = 1.3 W/(m^2·K)	Trap
Door	Constant heat flux, K = 1.6 W/(m^2·K)	Trap
Other walls and beds	Adiabatic, 0 W/m^2	Trap
Health care worker	Constant heat flux, 36.84 W/m^2	Trap
Patients	Constant heat flux, 42.11 W/m^2	Trap

2.2.2 Discrete phase

Table 1 lists the boundary conditions for the DPM. The droplet nuclei exhaled by the infector could be regarded as inert particles. Considering the low secondary load, the particle dispersion was modeled using Lagrangian approach. The one-way coupling was applied assuming that the effect of particles on airflow was negligible. The movement of particle could be described by Newton's second law, as given by Eq. (2). Exhaled particles were injected into the ward from the mouth of the injector (20 mm × 10 mm) at a constant rate. The pulmonary breathing volume rate of the injector was set as 6 L/min. The velocity and temperature of exhalation flow were 0.5 m/s and 35°C, respectively. Based on the actual particle diameter distribution generated during human breathing, the particles with ten different diameters (0.5 – 100 μm) were selected for this study. For the droplets with diameter of no more than 100 μm, the transient process of evaporation could be ignored [48]. The density of particles was 1026 kg/m^3. In a ventilated room, when the particles were in contact with solid surfaces, they were difficult to rebound to overcome adhesion. Therefore, "trap" condition was adopted to achieve particle deposition. For inlet and outlet, the boundary condition for DPM was set as "escape" [43]. The calculation terminated when particle reached vents or walls in the domain. "Enable node based averaging" was activated to consider the effect of the non-uniformity of discrete phase at the nodes. In this study, velocity fluctuation was defined as Gaussian distribution by the discrete random walk (DRW) model to consider the effect of turbulence, as defined by Eq. (3).

$$F_i = \frac{dv_{pi}}{dt} = \frac{18\mu}{\rho_p d_p^2}\frac{C_D Re}{24}\left(v_i - v_{pi}\right) + g\left(\frac{\rho_p - \rho}{\rho_p}\right) + F_a \quad (2)$$

Where F_i is the external forces exerted on the particle in i direction (m/s^2), v_{pi} is the velocity component

of particle in i direction (m/s), μ is the molecular viscosity of air (kg/(m·s)), ρ_p is the density of particle (kg/m^3), d_p is particle diameter (m), Re is Reynolds number, g is gravitational acceleration (m/s^2), and C_D is drag coefficient. In Eq. (2), the first, second and third terms on the right-hand side represent the drag force, the gravitational force and the additional forces exerted on a particle, respectively. The additional forces (F_a) in this study include Thermophoretic force, Brownian force and Saffman's lift force, and the details can be found in Reference [49].

$$v' = \varphi\sqrt{(\bar{v}')^2} = \varphi\sqrt{2k/3} \tag{3}$$

Where v' is the fluctuating component of air velocity (m/s), $\bar{v}$ is Reynolds-averaged air velocity (m/s), k is turbulent kinetic energy (m^2/s^2), and φ is normal distribution random number.

2.2.3 Independent tests

The computational domain was divided into hexahedral grids. Local refinement was performed for spaces with steep air velocity or temperature gradients. Four levels of mesh (1.79 million, 3.77 million, 5.80 million and 7.76 million) were used for independent test. The details were listed in Table 2. When the elements near the wall were not sufficiently refined, the kinetic energy of viscous sublayer might be over-predicted. This could enhance the velocity fluctuation and increase particle deposition [50]. Therefore, the predicted particle deposition fractions were compared before independent test. The deviation of the four meshes on particle deposition were less than 1%, indicating that grid thickness within the range of 6 – 15 mm was sufficient to describe the turbulence near walls. Then air temperature and velocity on the vertical centerline of the ward (X = 2.1 m, Y = 1.8 m) and the vertical line near the exterior wall (X = 0.1 m, Y = 1.8 m) were compared. The mesh with 7.76 million grids was selected as the reference, and the calculation errors of air temperature and velocity were quantified by the mean absolute error (MAE, as given by Eq. (4)). The prediction errors were listed in Table 2. Oversized grids filtered out more turbulence details and therefore coarse mesh performed poorly. The results showed that the air temperature and velocity predicted by 5.8 million grids were closest to the reference mesh. Therefore, the mesh with 5.8 million grids was selected for subsequent calculations. Fig. 2 shows the grid generation strategy for the hospital ward.

$$MAE = \frac{1}{n}\sum_{i=1}^{n}|y_i - x_i| \quad (4)$$

Where x_i is the reference value, y_i is the predicted value, and n is the number of sampling points.

Table 2 Grid details with different numbers.

Number of elements	Growth ratio	Thickness of the first layer element	Maximum grid width	MAE of air velocity	MAE of air temperature
1.79 million	1.0 – 1.5	15 mm	0.123	0.057 m/s	0.388°C
3.77 million	1.0 – 1.4	10 mm	0.086	0.028 m/s	0.214°C
5.80 million	1.0 – 1.4	8 mm	0.079	0.027 m/s	0.179°C
7.76 million	1.0 – 1.3	6 mm	0.051	-	-

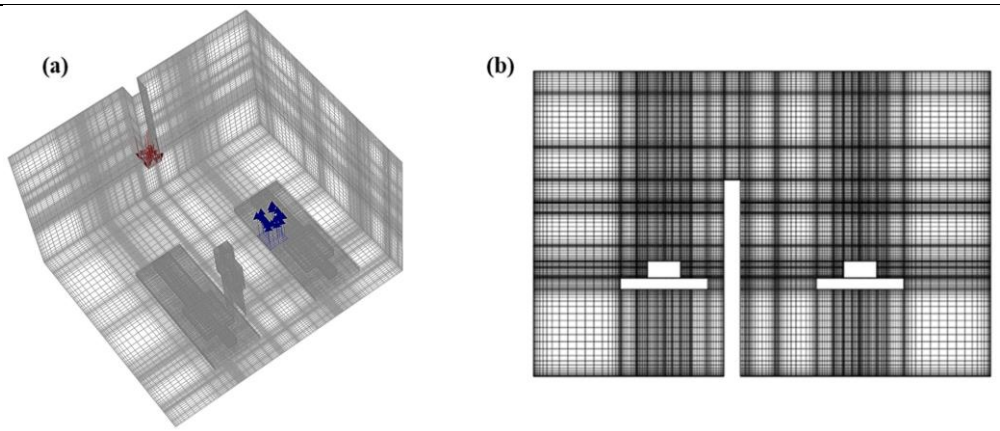

Fig. 2 Mesh for the simulated hospital ward. (a) 3D schematic, (b) Cross section (Y = 2.6 m).

To avoid statistical distortion, an independent test for the number of released particles was performed. Six different particle numbers (i.e., 10000, 20000, 30000, 40000, 50000 and 60000) were checked. The case with particle number of 60000 was selected as the reference. The suspension, deposition and removal fractions defined by Eq. (5), (6) and (7) were compared, respectively. When the number of released particles exceeded 50000, the deviations of all the three components were less than 1% concurrently. Therefore, at least 50000 particles were exhaled from the infector in each case.

$$\eta_{suspension} = \frac{n_{suspension}}{n_{total}} \times 100\% \quad (5)$$

$$\eta_{deposition} = \frac{n_{deposition}}{n_{total}} \times 100\% \quad (6)$$

$$\eta_{removal} = \frac{n_{removal}}{n_{total}} \times 100\% = 1 - \left(\eta_{suspension} + \eta_{deposition}\right) \quad (7)$$

Where $\eta_{suspension}$, $\eta_{deposition}$ and $\eta_{removal}$ are particle suspension fraction, deposition fraction and removal fraction, respectively. n_{total} is the total number of particles exhaled by the infector, $n_{suspension}$ is the

number of particles suspended in indoor air, $n_{deposition}$ is the number of particles deposited on the solid surfaces, and $n_{removal}$ is the number of particles removed by the exhaust air outlet.

2.3 Validations for numerical simulation

To validate the accuracy of RNG *k*-ε model in predicting the airflow field under IJV in heating mode, the experimental data measured by Ye et al. [51] was selected as the reference. The data was collected in a test chamber with dimensions of 3600 mm × 3000 mm × 2600 mm (see Fig. 3). A circular nozzle (200 mm diameter) as the supply air inlet was installed on the wall to provide warm air. The height of inlet was 170 mm above the floor. The supply air temperature and velocity were 35.6°C and 1.2 m/s, respectively. Indoor air was exhausted by an outlet located on the ceiling. The dimensions of the outlet were 200 mm × 300 mm. Detailed boundary conditions could be found in Reference [51]. The simulated and measured results along four vertical Sampling Lines S1 – S4 were compared, as shown in Fig. 4. The results calculated by RNG *k*-ε model matched the measured data well. MAE was used to quantify the deviation between experimental and simulated results. The MAE values of normalized air velocity and temperature were 0.025 and 0.041, respectively. Therefore, the RNG *k*-ε model could be used to predict the airflow of IJV in heating mode.

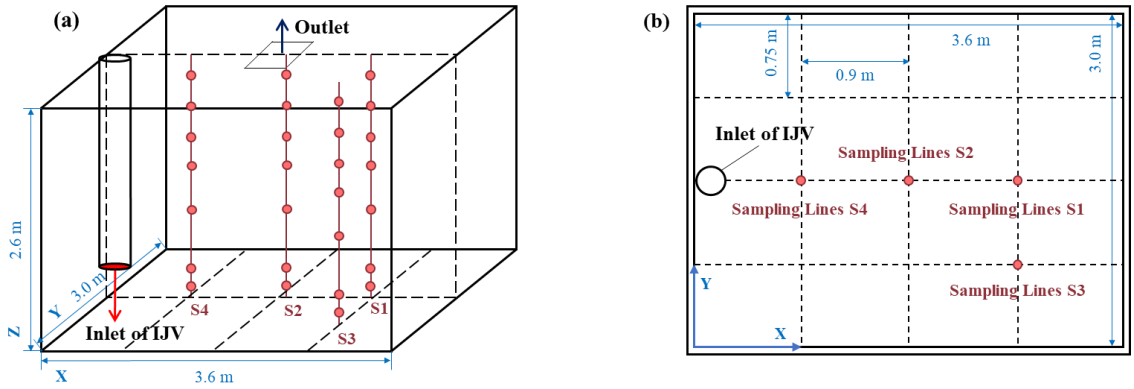

Fig. 3 (a) Experimental layout, (b) Plan of the test chamber [51].

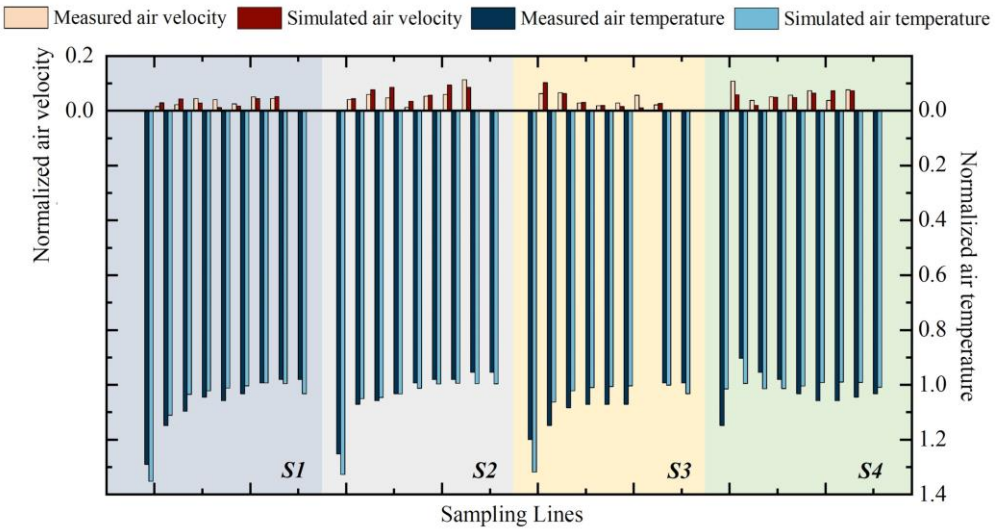

Fig. 4 Comparison of normalized air temperature and velocity between experiment and simulation.

Based on the particle concentration data from Chen et al. [52], the prediction accuracy of DPM was validated. The experiments were conducted in a test chamber with dimensions of 800 mm × 400 mm × 400 mm (see Fig. 5). The particles were injected into the chamber along with supplied air at a velocity of 0.225 m/s. The average diameter of injected particles was 10 μm. The density of particles was 1400 kg/m^3. Details for the experiment and its boundary conditions could be found in Reference [52]. Fig. 6 shows the comparison results of particle concentration along three vertical Sampling Lines between experiment and simulation. The predicted results exhibited a similar variation trend to the measured data. The MAE value of normalized particle concentration was 0.112, indicating that the DPM could provide a good prediction performance for particle dispersion.

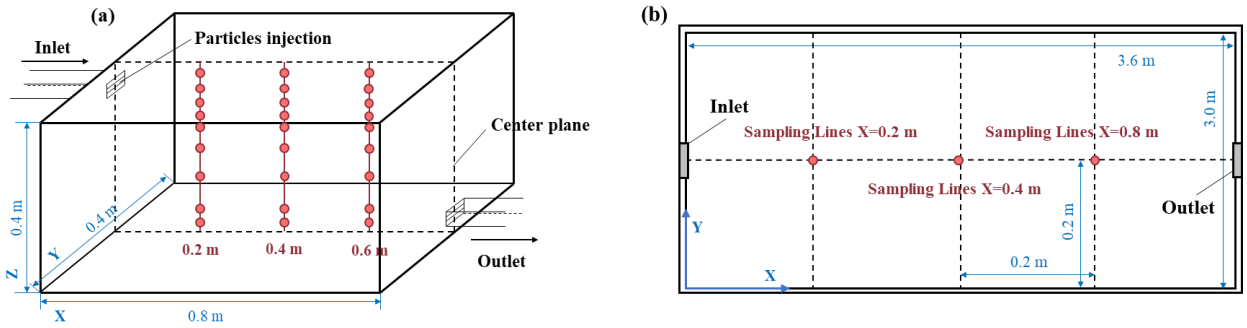

Fig. 5 (a) Experimental layout, (b) Plan of the test chamber [52].

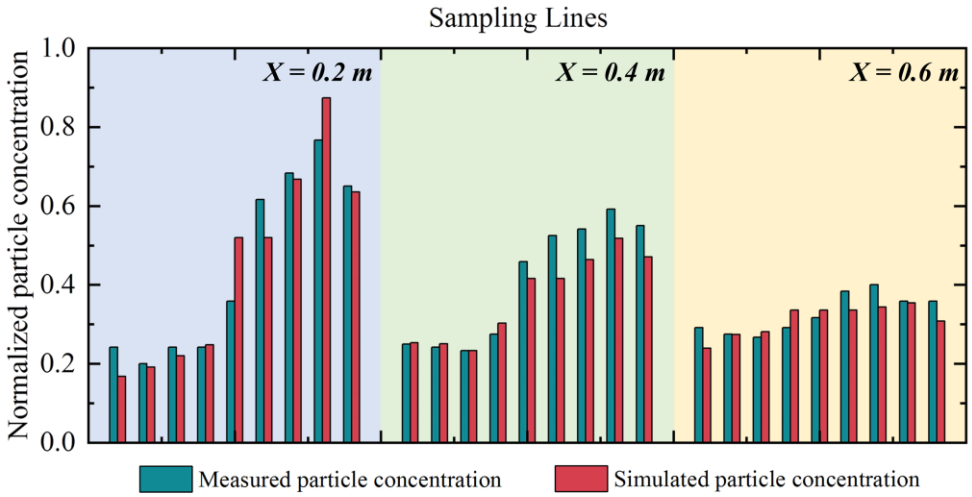

Fig. 6 Comparison of normalized particle concentration between experiment and simulation.

Under the same boundary conditions, indoor concentration distributions for constant and periodic breathing modes were compared. The average mass flow rate of exhalation was set at 6×10^{-18} kg/min. For periodic breathing mode, each breathing cycle consisted of 2.5 s of inhalation, 1.0 s of pause, and 2.5 s of exhalation. The peak velocity at infector's mouth was 0.5 m/s, which was consistent with the constant exhalation. The periodic breathing frequency of the infector was 10 times/min [53]. By comparing normalized particle concentration (normalized using exhausted particle concentration) near the supply air inlet (L1, X = 2.1 m, Y = 0.5 m), the centerline of the room (L2, X = 2.1 m, Y = 1.7 m), and the exhaust outlet (L3, X = 2.1 m, Y = 3.2 m), the differences between different breathing modes were compared. The results are shown in Fig. 7. The transient simulation for periodic breathing was performed after the airflow field stabilizing. The concentration on the three lines were calculated as the average value during three breathing cycles after 15 minutes. The comparison results showed that the distribution trends of particle concentration under the two breathing modes were similar. The MAE value of normalized particle concentration was 0.233. Since large errors were only found in local zones close to the infector, it could be considered that simplified constant breathing mode was feasible. This simplified method was also used by Zhou et al. [54] for the study of lock-up phenomenon of exhaled flow. Wang et al. [39] studied exhaled particle dispersion under MV and IJV based on this assumption.

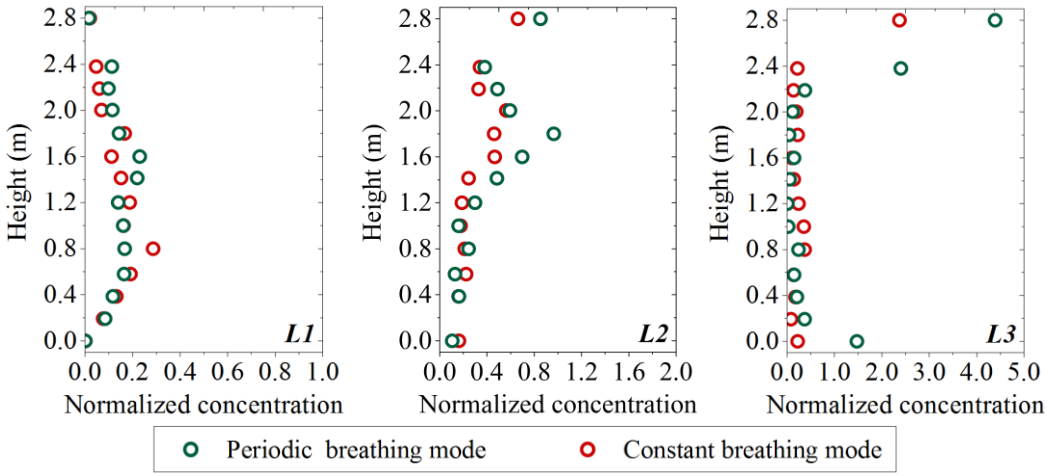

Fig. 7 Comparison of normalized particle concentration between periodic and constant breathing modes.

3. Results and discussion

3.1 Effect of supply air parameters on particle dispersion

Understanding the effects of supply air parameters on particle dispersion can help promote the application of IJV in hospital wards. Since the inlet of IJV was close to the occupied zone, the supply air parameters could significantly affect indoor airflow pattern and exhaled particle dispersion. To analyze the effect of supply air parameters on particle dispersion, different levels of air changes per hour (*ACH*) and supply air temperature (T_s) were used as variables, as shown in Table 3. Cases 1 – 16 were specified by the full factorial design method to provide comprehensive information and consider their impact of interaction. The selection of parameters was based on requirements for hospital ward and common values set in heating applications under IJV. The *ACH* was in the range of 6 – 15 h^{-1}, and the T_s was in the range of 24 – 30°C. The infector location (*IL*) was defined as Patient 2 close to the health care worker (see Fig. 1). The outdoor air temperature (T_{out}) was set as 2.2°C. The corresponding heat fluxes for the exterior wall, window, right wall and door were -20.8 W/m^2, -62.4 W/m^2, -18.9 W/m^2 and -31.6 W/m^2, respectively. The average indoor air temperatures of Cases 1 – 16 were above 20°C. The initial Reynolds numbers (*Re*) of the simulated cases were above 20000, indicating that the flow in the ward was turbulent. The effects of different relative magnitudes of thermal buoyancy and inertia force were considered, the initial Archimedes numbers (*Ar*) ranged between 0.001 and 0.03. For all cases, the vertical air temperature differences between the head and ankle levels of occupants were lower than 3°C. At the height of head, the draft rates were lower than 10%.

Table 3 Simulated cases by a full factorial design method.

Case	T_s (°C)	ACH (h^{-1})	IL	T_{out} (°C)	Re	Ar
1	24.0	6	2	2.2	21633	0.0260
2	26.0	6	2	2.2	21372	0.0294
3	28.0	6	2	2.2	21133	0.0287
4	30.0	6	2	2.2	20886	0.0290
5	24.0	9	2	2.2	32545	0.0088
6	26.0	9	2	2.2	32153	0.0086
7	28.0	9	2	2.2	31793	0.0085
8	30.0	9	2	2.2	31421	0.0086
9	24.0	12	2	2.2	43074	0.0035
10	26.0	12	2	2.2	42555	0.0036
11	28.0	12	2	2.2	42079	0.0035
12	30.0	12	2	2.2	41586	0.0034
13	24.0	15	2	2.2	53603	0.0018
14	26.0	15	2	2.2	52957	0.0018
15	28.0	15	2	2.2	52365	0.0017
16	30.0	15	2	2.2	51752	0.0017

Fig. 8 shows the particle concentration distributions at typical T_s (24°C and 26°C) and ACH (9 h^{-1} and 12 h^{-1}). The reference planes were selected as X = 3.0 m and Y = 3.3 m passing through the infector's mouth. As shown in Fig. 8(a2), when T_s was low (24°C), exhaled particles had an evident trend of horizontal dispersion under the influence of asymmetrical heat loss between exterior and internal enclosures. Horizontally moving particles could deteriorate the inhaled air quality of the health care worker and Patient 1. After the increase of T_s from 24°C to 26°C, particles could be observed moving towards the upper zone of the ward, as shown in Fig. 8(b). Combining the results of indoor airflow field (Fig. 9(a) and (b)), it was found that increasing T_s elevated the air temperature of the room. The supply airflow of IJV was transported directly downwards to the bottom of the ward, so the high-temperature supply air had a stronger rising tendency. Within a sufficient air supply distance, the warm air can carry more particles into the upper zone of the ward. The similar results were reported by Jurelionis et al. [55] in their experiments with radiant floor heating system.

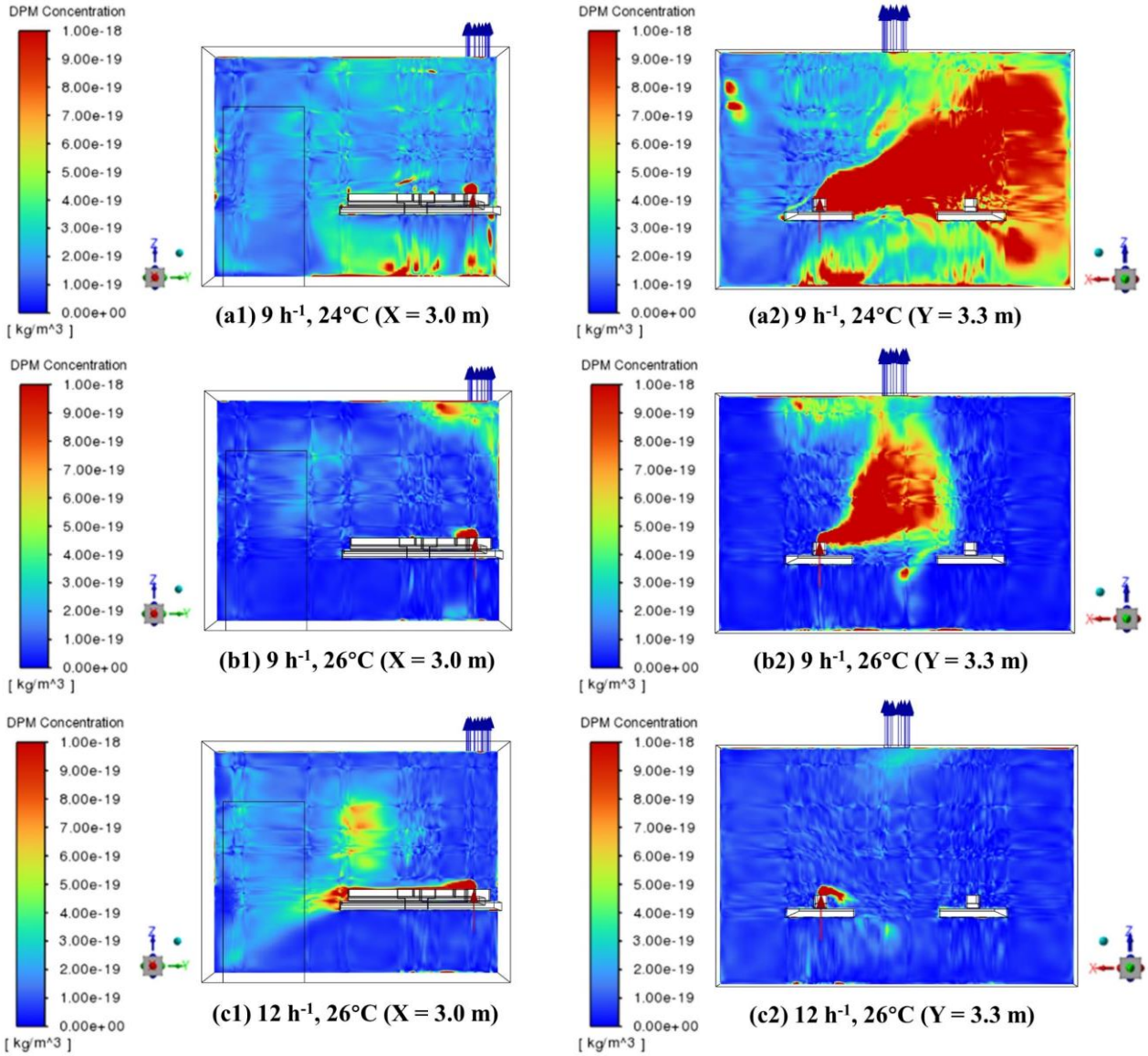

Fig. 8 Comparison of particle concentration distributions under different supply air parameters. (a) 9 h^{-1}, 24°C, (b) 9 h^{-1}, 26°C, (c) 12 h^{-1}, 26°C.

Fig. 8(b) and (c) show the particle concentration distributions under two typical *ACH* conditions (9 h^{-1} and 12 h^{-1}). On the one hand, the increased supply airflow rate diluted the particle concentration in the occupied zone, as shown in Fig. 8(b2) and (c2). On the other hand, the higher *ACH* enhanced indoor air mixing, thus some particles moved towards the supply air inlet, as shown in Fig. 8(b1) and (c1). Combining the results of indoor airflow field, when T_s was 26°C and *ACH* was 9 h^{-1}, the warm airflow of IJV could comply with the direction of human body plume and exhalation flow. After *ACH* increased, the air velocity in the occupied zone was increased and the spreading distance of warm air was extended. More fresh air entered into the occupied zone, resulting in the dilution of particle concentration. It was noted that the high-velocity air supply changed the direction of air flow near the

patient and therefore caused more particles to be sucked into the supply air jet. For the controlled environment, this phenomenon was undesirable as some particles may remain indoors for long periods of time [56]. The particle concentration results indicated that both T_s and *ACH* could affect particle dispersion.

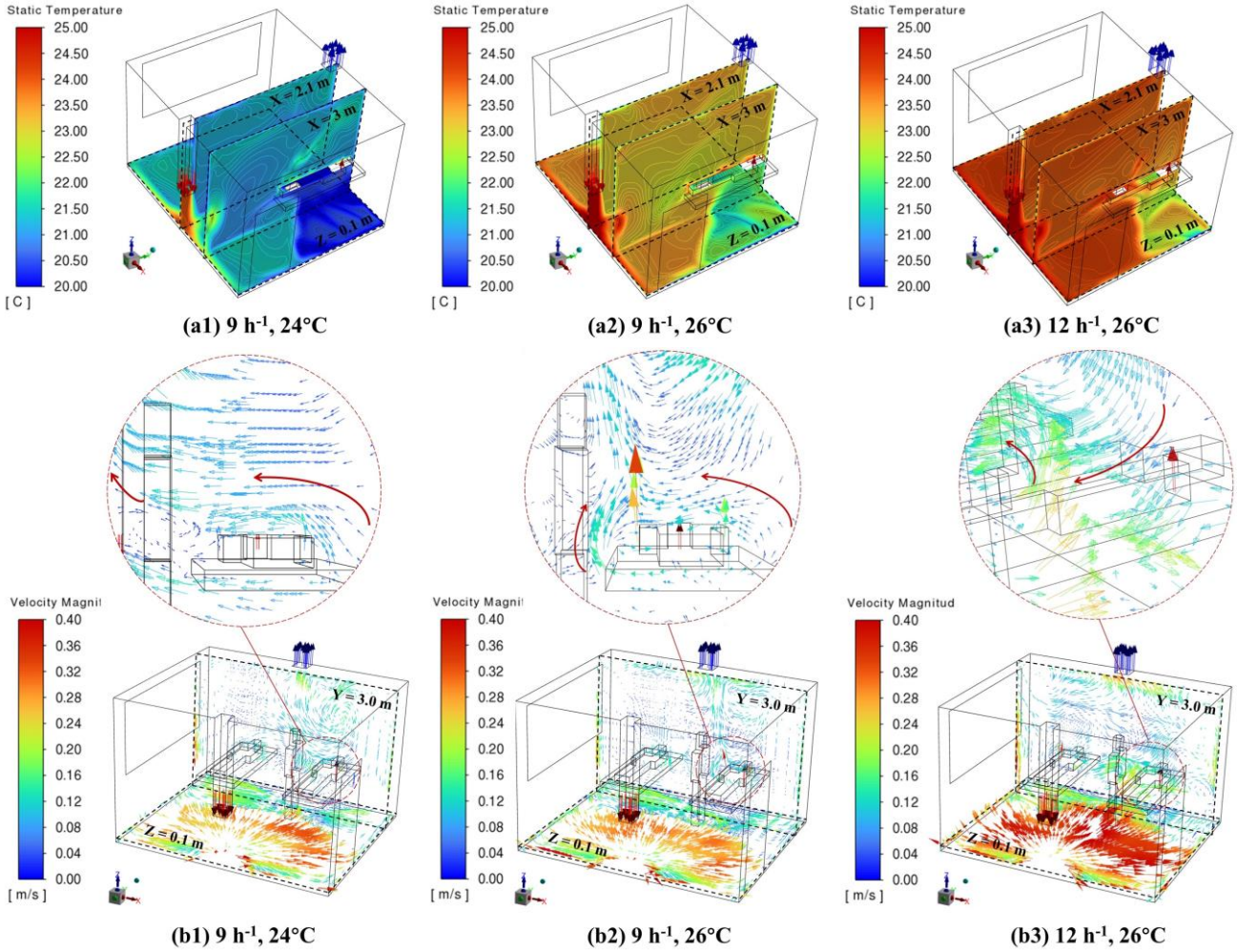

Fig. 9 Comparison of (a) air temperature distribution and (b) air velocity distribution under different supply air parameters.

To quantitatively analyze the effect of supply air parameters on particle dispersion, the suspension, deposition and removal fractions of particles under different T_s and *ACH* were calculated, as shown in Fig. 10. The darker grid color represented a larger percentage. As shown in Fig. 10(a), with the increase of T_s, the removal fraction of fine particles (diameter ≤ 20 μm) exhibited an evident increasing tendency, the deposition fraction exhibited an evident decreasing tendency, and the suspension fraction did not change significantly. When T_s was increased from 24°C to 30°C, the removal fractions of 0.5 μm, 1 μm, 5 μm, 10 μm and 20 μm particles increased by 38.60%, 38.73%, 38.80%, 44.60% and

56.67%, respectively, while the deposition fractions decreased by 26.87%, 27.08%, 28.33%, 38.71% and 55.29%, respectively. The particle fates matched the results of particle concentration distribution.

As shown in Fig. 10(b), there was not a linear relationship between the *ACH* and particle fates. With the increase in *ACH*, the removal fraction of fine particles increased and then decreased, while the variation of the deposition and suspension fractions of fine particles were contrary. When *ACH* was increased from 6 h^{-1} to 9 h^{-1} (T_s = 26°C), the removal fractions of 0.5 μm, 1 μm, 5 μm, 10 μm and 20 μm particles increased by 20.78%, 20.66%, 19.04%, 19.52% and 29.35%, respectively, while the suspension fractions decreased by 14.11%, 13.55%, 10.83%, 8.41% and 12.41%, respectively. This was because the warm airflow of IJV could fit well with the human body plume and exhalation flow under an appropriate combination of supply air parameters. In this case, the warm air near the floor could transport more fine particles to the ceiling. When *ACH* was further increased, the air velocity in the occupied zone increased, resulting in an increased probability of particles contacting solid surfaces. When *ACH* was increased from 9 h^{-1} to 15 h^{-1}, the deposition fractions of 0.5 μm, 1 μm, 5 μm, 10 μm and 20 μm particles increased by 35.07%, 35.91%, 37.35%, 43.30% and 41.70%, respectively. Additionally, the elevated *ACH* enhanced the entrainment effect for fine particles. The probability of fine particles staying in indoor air and the suspension fractions were increased. When *ACH* was increased from 9 h^{-1} to 15 h^{-1}, the suspension fractions of 0.5 μm, 1 μm, 5 μm and 10 μm particles increased by 13.52%, 13.83%, 11.79% and 4.68%, respectively.

When particle diameter was large, the influence of supply airflow on particle dispersion was minimal, as the gravity of particle dominated its dispersion [13]. Therefore, for medium (30 – 50 μm) and coarse (> 50 μm) particles, their deposition fractions exceeded 90% under all supply air parameters.

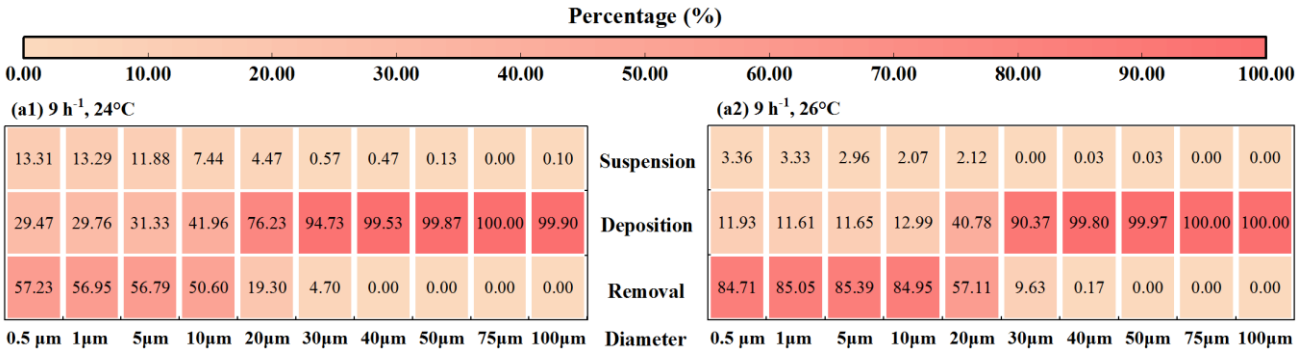

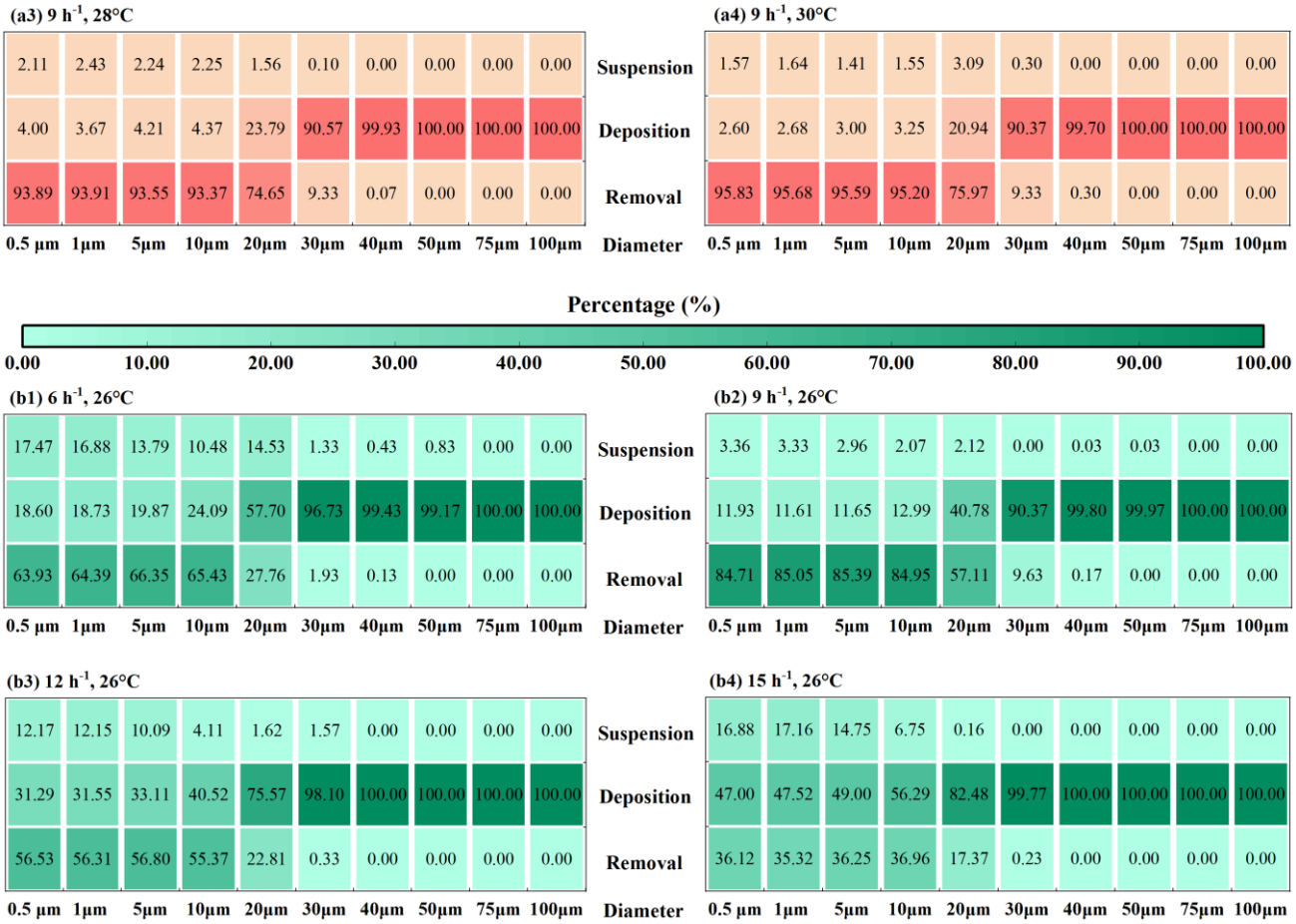

Fig. 10 Comparison of particle dispersal behaviors under (a) different supply air temperatures and (b) different air changes per hour.

Fine particles are the main carriers for airborne transmission. Fig. 11 shows the trajectories and the residence times of 5 μm particles under different T_s (24°C and 26°C) and *ACH* (9 h^{-1} and 12 h^{-1}). At a low T_s (24°C), fine particles moved horizontally after being exhaled from the infector. It could be found only a small amount of fine particles were exhausted by the ceiling outlet. After an increase in T_s, the average travelling distance of fine particles in the ward was shortened evidently. Moreover, more fine particles could be removed, as shown in Fig. 11(b). When *ACH* rose to 12 h^{-1}, the increase in *ACH* enhanced air mixing and accelerated the movement of fine particles in the occupied zone. The average residence time of fine particles was shortened. Meanwhile, it could be observed that the supply airflow of IJV entrained fine particles, which led to a decrease in the removal and an increase in the travelling distance of fine particles.

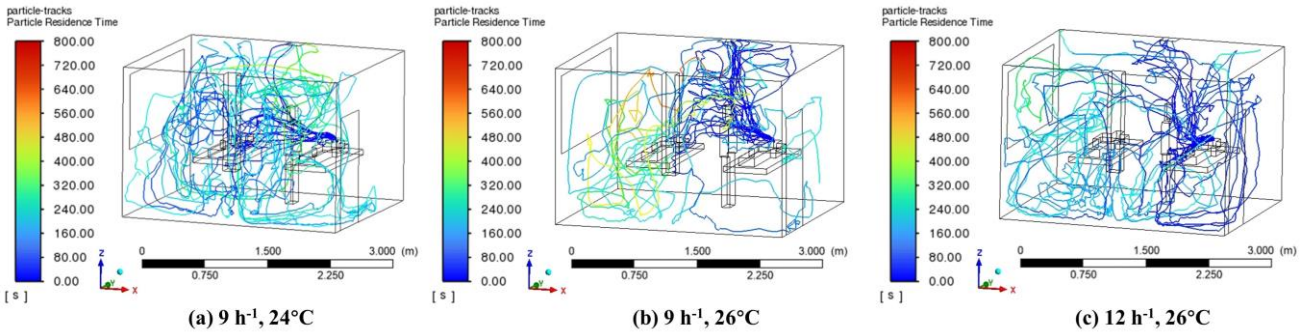

Fig. 11 Comparison of 5 μm particle residence time and trajectories under different supply air parameters. (a) 9 h^{-1}, 24°C, (b) 9 h^{-1}, 26°C, (c) 12 h^{-1}, 26°C.

Fig. 12(a) and (b) show the variation patterns of average removal fraction ($\eta_{R,fp}$) and average deposition fraction of fine particles ($\eta_{D,fp}$) for Cases 1 – 16, respectively. With the increase in *ACH*, $\eta_{R,fp}$ increased and then decreased. With the increase in T_s, $\eta_{R,fp}$ increased, but the growth gradient gradually slowed down. Meanwhile, with the increase in *ACH*, $\eta_{D,fp}$ decreased and then increased. With the increase in T_s, $\eta_{D,fp}$ decreased, but the decay gradient gradually slowed down. The second-order fitting model was used to model the correlation between particle elimination and supply air parameters, as given by Eq. (8) and (9).

$$\eta_{R,fp} = -0.0072ACH^2-0.0045ACH\cdot T_s-0.0056T_s^2+0.2352ACH+0.3858T_s-6.0379,\ R^2 = 0.823 \quad (8)$$

$$\eta_{D,fp} = 0.004ACH^2+0.0032ACH\cdot T_s+0.0066T_s^2-0.1329ACH-0.4187T_s+6.8028,\ R^2 = 0.824 \quad (9)$$

Where $\eta_{R,fp}$ is the average removal fraction of fine particles, $\eta_{D,fp}$ is the average deposition fraction of fine particles.

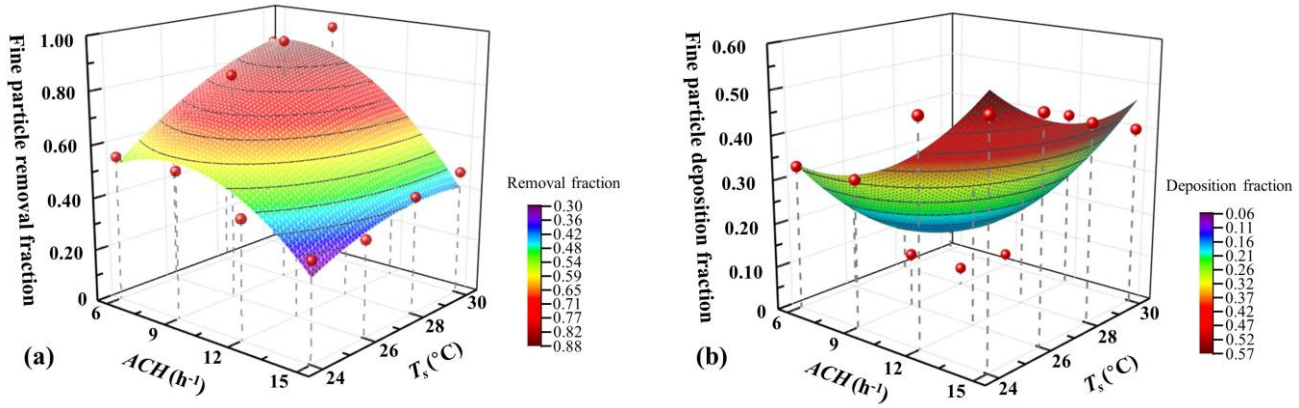

Fig. 12 Variation of particle elimination with supply air parameters. (a) Particle removal, (b) Particle deposition.

The prediction capabilities of the correlation models were satisfactory, with the determination

coefficient (R^2) values higher than 0.80. From the regression equations, it could be found that the *ACH* had a more significant effect on particle dispersion, and therefore *ACH* should be prioritized in the design of IJV heated wards. The established correlation models can help environmental managers to quickly identify the main elimination way of fine particles in the ward, and to take some targeted interventions (e.g. air disinfection, surface wiping, etc.).

3.2 Factor impact analysis

3.2.1 Response indicators and the results of orthogonal design cases

Using orthogonal design method, Cases 17 – 32 considered the effects of two uncontrollable factors. The purpose was to judge the ability of supply air parameters to influence particle dispersion and to improve reliability in subsequent optimization (Section 3.3). Factor A and Factor B were T_s and *ACH*, respectively. Four levels of each factor were selected to cover common supply air conditions of IJV in winter. Factor C and Factor D were uncontrollable parameters. Factor C was selected as two levels, representing two different *IL* in the two-bed hospital ward. Factor D was T_{out}, and four levels were chosen. The levels of Factor D covered common outdoor air temperature and an extreme air temperature during winter in Chongqing, China. Factor E was the error (blank column), it was used to perform the error analysis. $L_{16}(4^3 \times 2^1)$ orthogonal table was used to design the simulated cases. A total of sixteen cases (Cases 17 – 32) were specified, as listed in Table 4. $\eta_{removal}$ (defined by Eq. (7)) and the average particle residence time (τ, calculated by CFD Post software) were selected as the response indicators to judge the effect of particle control at spatial and temporal aspects, respectively. A larger $\eta_{removal}$ indicates a smaller particle load inside the ward. Additionally, τ is longer, implying that particles follow indoor air for a longer period of time. The calculated results for the two indicators were also summarized in Table 4.

Table 4 Studied cases determined by orthogonal design and simulated results.

Case	Factor					Combination	$\eta_{removal}$ (%)	τ (s)
	A	B	C	D	E			
17	24°C	9 h^{-1}	1	2°C	2	$A_1B_2C_3D_1E_2$	34.64	76
18	28°C	15 h^{-1}	1	10°C	2	$A_3B_4C_1D_1E_2$	26.33	68
19	26°C	15 h^{-1}	2	2°C	3	$A_2B_4C_3D_2E_3$	29.69	57

20	30°C	9 h^{-1}	2	10°C	3	$A_4B_2C_1D_2E_3$	67.07	119
21	24°C	12 h^{-1}	2	10°C	4	$A_1B_3C_1D_2E_4$	31.66	77
22	28°C	6 h^{-1}	2	2°C	4	$A_3B_1C_3D_2E_4$	37.96	229
23	26°C	6 h^{-1}	1	10°C	1	$A_2B_1C_1D_1E_1$	55.83	183
24	30°C	12 h^{-1}	1	2°C	1	$A_4B_3C_3D_1E_1$	35.82	91
25	24°C	6 h^{-1}	2	-2°C	3	$A_1B_1C_4D_2E_3$	22.99	98
26	28°C	12 h^{-1}	2	6°C	3	$A_3B_3C_2D_2E_3$	46.20	62
27	26°C	12 h^{-1}	1	-2°C	2	$A_2B_3C_4D_1E_2$	32.47	70
28	30°C	6 h^{-1}	1	6°C	2	$A_4B_1C_2D_1E_2$	57.93	153
29	24°C	15 h^{-1}	1	6°C	1	$A_1B_4C_2D_1E_1$	25.90	48
30	28°C	9 h^{-1}	1	-2°C	1	$A_3B_2C_4D_1E_1$	63.94	57
31	26°C	9 h^{-1}	2	6°C	4	$A_2B_2C_2D_2E_4$	59.71	73
32	30°C	15 h^{-1}	2	-2°C	4	$A_4B_4C_4D_2E_4$	25.75	53

3.2.2 Range analysis

Range analysis was used to determine the primary and secondary order of factors. The results of the range analysis are given in Table 5. The mean value of the response indicator corresponding to Factor i at Level j (k_{ij}) was calculated by Eq. (10). The range value of Factor i (R_i) was calculated by Eq. (11). The larger the value of R_i, the greater the effect of Factor i on the response indicator.

$$k_{ij} = \frac{1}{l}\sum_{j=1}^{l} x_{ij} \quad (10)$$

$$R_i = k_{ij,max} - k_{ij,min} \quad (11)$$

Where x_{ij} is the value of the response indicator for Factor i at Level j, l is the total number of levels for Factor i, $k_{ij,max}$ is the maximum mean value of the indicator at each level for Factor i, and $k_{ij,min}$ is the minimum mean value of the indicator at each level for Factor i.

Table 5 Results of range analysis.

Indicator	Range values	Factor				
		A	B	C	D	E (Error)
$\eta_{removal}$ (%)	k_{i1}	28.80	43.68	41.61	45.22	45.37
	k_{i2}	44.43	56.34	40.13	47.44	37.84
	k_{i3}	43.61	36.54	-	34.53	41.49
	k_{i4}	46.64	26.92	-	36.29	38.77

	R_1	17.85	29.42	1.48	12.91	7.53
	k_{i1}	74.77	165.80	93.23	111.64	94.73
	k_{i2}	95.83	81.04	95.92	83.97	91.73
τ (s)	k_{i3}	103.79	74.91	-	113.42	83.90
	k_{i4}	103.90	56.55	-	69.28	107.93
	R_2	29.13	109.24	2.69	44.14	24.03

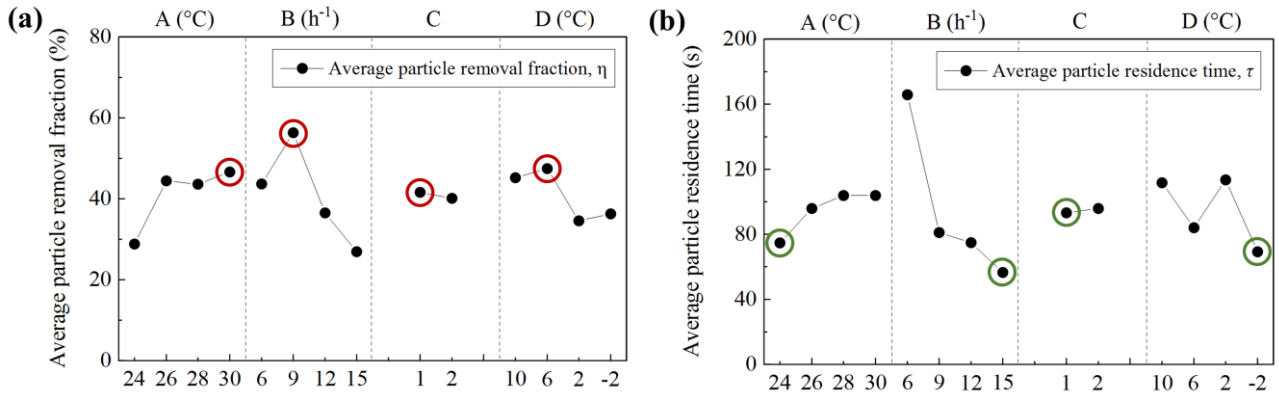

Fig. 13 Mean values of each level of factors. (a) Using $\eta_{removal}$ as the response indicator, (b) Using τ as the response indicator.

When $\eta_{removal}$ was used as the response indicator, the influencing factors in descending order of R-value were *ACH* (29.42) > T_s (17.85) > T_{out} (12.91) > *IL* (1.48). Fig. 13(a) showed the mean values of each factor at each level when $\eta_{removal}$ was the response indicator. The maximum or minimum mean value of the response indicator determined a recommended level of the factor. For $\eta_{removal}$, a larger value was preferred. As shown in Fig. 13(a), the optimal levels of parameters were highlighted in red circles. It could be found that the recommended combination of supply air parameters was A_4B_2, with T_s of 30°C and *ACH* of 9 h^{-1}. When τ was used as the response indicator, the influencing factors in descending order of R-value were *ACH* (109.24) > T_{out} (44.14) > T_s (29.13) > *IL* (2.69). Fig. 13(b) showed the mean values of each factor at each level when τ was the response indicator. For τ, a smaller value was preferred. As shown in Fig. 13(b), the optimal levels of parameters were highlighted in green circles. It could be found that the recommended combination of supply air parameters was A_1B_4, with T_s of 24°C and *ACH* of 15 h^{-1}.

3.2.2 Analysis of variance

The analysis of variance (ANOVA) was conducted, with the aim of determining the significance and contribution of each factor. Table 6 lists the results of ANOVA.

Table 6 Results of ANOVA.

Indicator	Source	Sum of squares	Degree of freedom	Mean square	F-value	P-value	Contribution	Significance
$\eta_{removal}$ (%)	Factor A	796.89	3	265.63	5.82	0.09	23.07%	-
	Factor B	1842.82	3	614.27	13.47	0.03	53.35%	√
	Factor C	8.75	1	8.75	0.19	0.69	0.25%	-
	Factor D	493.28	3	164.43	3.61	0.16	14.28%	-
	Error E	136.81	3	45.60				
τ (s)	Factor A	2262.54	3	754.18	1.88	0.31	5.63%	-
	Factor B	28353.55	3	9451.18	23.59	0.01	70.55%	√
	Factor C	28.89	1	28.89	0.07	0.81	0.07%	-
	Factor D	5593.44	3	1864.48	4.65	0.12	13.92%	-
	Error E	1201.72	3	400.57				

The multi-factor ANOVA was used to investigate the effects of T_s, ACH, IL and T_{out} for $\eta_{removal}$. The R^2 value of the model was 0.91, indicating that these four factors could explain 91% of the changes of $\eta_{removal}$. From Table 6, it could be seen that the ACH was the most influential factor on $\eta_{removal}$ with a contribution percentage of 53.35%, followed by T_s (23.07%), T_{out} (14.28%) and then IL (0.25%). A higher F-value indicated a more significant effect of the factor on the response indicator. To determine the statistical significance of factor, P-value (< 0.05) was used to estimate whether the F-value was large enough. The results showed that ACH had a significant effect on $\eta_{removal}$ (P = 0.03), and the effect of T_s was marginally significant (P = 0.09). The multi-factor ANOVA was used to investigate the effects of four factors on τ. The R^2 value of the model was 0.9, indicating that these four factors could explain 90% of the changes of τ. The order of the four factors affecting τ was as follows, $ACH > T_{out} > T_s > IL$. The contribution percentages of ACH, T_{out}, T_s and IL were 70.55%, 13.92%, 5.63% and 0.07%, respectively. Meanwhile, the results in Table 6 showed that ACH was statistically significant (P = 0.01). The results of ANOVA showed that the total contribution percentages of supply air parameters (i.e., T_s

and *ACH*) to the variation of $\eta_{removal}$ and τ were 76.42% and 76.18%, respectively. The above results showed the importance of reasonable selection for supply air parameters in the ward heated by IJV.

3.3 Grey relational multi-objective optimization

From the results of range analysis, for two different response indicators, the optimal combinations of supply air parameters were different. Therefore, grey relational analysis was used to transform the problem from bi-objective to single objective. Grey relational optimization was performed based on following steps.

Step 1: Normalize the results of response indicators.

For the benefit indicator, $\eta_{removal}$, as normalized by Eq. (12).

$$x_i(j) = \frac{x_{ij} - min\{x_{ij}\}}{max\{x_{ij}\} - min\{x_{ij}\}} \tag{12}$$

For the cost-type indicator, τ, as normalized by Eq. (13).

$$x_i(j) = \frac{max\{x_{ij}\} - x_{ij}}{max\{x_{ij}\} - min\{x_{ij}\}} \tag{13}$$

Where $x_i(j)$ is the normalized value of the response indicator, x_{ij} is the value of the response indicator, $max\{x_{ij}\}$ is the maximum value of the response indicator, $min\{x_{ij}\}$ is the minimum value of the response indicator, i represents the ith case (i = 1, 2, ..., a), and j represents the jth response indicator (j = 1, 2, ..., b). In this study, a = 16 and b = 2.

Step 2: Establish the analysis sequence, as given by Eq. (14).

$$(X_0, X_1, \cdots, X_i) = \begin{pmatrix} x_0(1) & \cdots & x_i(1) \\ \vdots & \ddots & \vdots \\ x_0(j) & \cdots & x_i(j) \end{pmatrix}_{j \times (i+1)} \tag{14}$$

Where X_0 is the normalized reference sequence, which is assumed to be 1 [57].

Step 3: Solve for the grey correlation coefficient, as defined by Eq. (15).

$$\xi_{0,i}(j) = \frac{\Delta_{min} + \xi\Delta_{max}}{\Delta_{0,i}(j) - \xi\Delta_{max}} \tag{15}$$

Where $\xi_{0,i}(j)$ is the grey correlation coefficient of the jth response indicator, ξ is the distinguishing coefficient, which is taken as 0.5 [58], Δ_{min} is the minimum value in the deviation sequence, and Δ_{max} is the maximum value in the deviation sequence.

Step 4: Establish the sequence of grey relational coefficient, as given by Eq. (16).

$$\left(\xi_{0,1},\xi_{0,2},\cdots,\xi_{0,i}\right)=\begin{pmatrix}\xi_{0,1}(1) & \cdots & \xi_{0,i}(1)\\ \vdots & \ddots & \vdots\\ \xi_{0,1}(j) & \cdots & \xi_{0,i}(j)\end{pmatrix}_{j\times i} \tag{16}$$

Step 5: Calculate the grey relational grade (*GRG*) for each case, as given by Eq. (17).

$$GRG_i=\frac{1}{n}\sum_{j=1}^{n}\xi_{0,i}(j) \tag{17}$$

Where GRG_i is the grey relational grade for the *i*th case. *GRG* can reflect the consistency trend among two factors. The higher *GRG* was, the closer the tested parameter to the ideal parameter.

Table 7 Results of grey relational multi-objective optimization.

Case	$\eta_{removal}$ (%)	τ (s)	Normalized η	Normalized τ	$\xi_{0,i}(1)$	$\xi_{0,i}(2)$	*GRG*
17	34.64	76	0.26	0.85	0.40	0.77	0.586
18	26.33	68	0.08	0.89	0.35	0.82	0.586
19	29.69	57	0.15	0.95	0.37	0.91	0.640
20	67.07	119	1.00	0.61	1.00	0.56	0.781
21	31.66	77	0.20	0.84	0.38	0.76	0.571
22	37.96	229	0.34	0.00	0.43	0.33	0.382
23	55.83	183	0.75	0.25	0.66	0.40	0.533
24	35.82	91	0.29	0.76	0.41	0.68	0.544
25	22.99	98	0.00	0.72	0.33	0.64	0.487
26	46.20	62	0.53	0.93	0.51	0.88	0.696
27	32.47	70	0.22	0.88	0.39	0.81	0.599
28	57.93	153	0.79	0.42	0.71	0.46	0.584
29	25.90	48	0.07	1.00	0.35	1.00	0.675
30	63.94	57	0.93	0.95	0.88	0.91	0.893
31	59.71	73	0.83	0.86	0.75	0.78	0.764
32	25.75	53	0.06	0.97	0.35	0.94	0.645
Mean	40.87	95					

Table 7 lists the results of *GRG* for Cases 17 – 32. The results showed that Case 22 (i.e., $A_3B_1C_3D_2$) had the worst performance, with the smallest *GRG* value of 0.382. Case 30 (i.e., $A_3B_2C_4D_1$) had the highest *GRG* value (0.893), implying that Case 30 provided the optimal combination of supply air

parameters considering maximum $\eta_{removal}$ and minimum τ concurrently. The corresponding ACH and T_s were 9 h^{-1} and 28°C, respectively, with $\eta_{removal}$ as high as 63.94% and τ as low as 57 s. The average $\eta_{removal}$ and τ of Cases 17 – 32 were calculated and listed in Table 7. Compared to the mean values, $\eta_{removal}$ was elevated by 23.07% and τ was lowered by 38 s under this optimal operating condition. The velocity vector for Case 30 was shown in Fig. 14(a). It could be seen that the supply airflow of IJV was effectively transported to the occupied zone and complied with the human body plume. Under the interaction between the supply airflow and human body plume, the particles exhaled from the infector exhibited an evident upward movement, and then were removed through the ceiling outlet, as shown in Fig. 14(b). As a result, the particle load remaining in indoor air was low under the optimal supply air parameters.

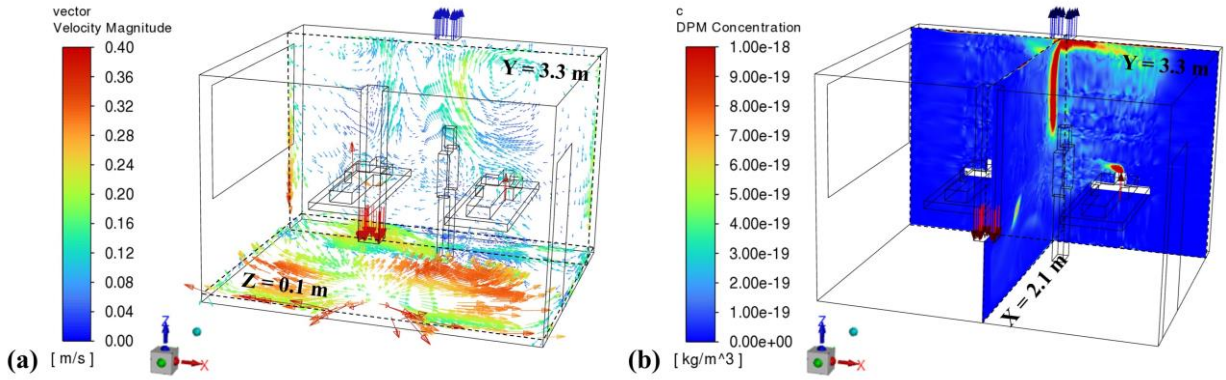

Fig. 14 Numerical simulation results of the optimal case. (a) Air velocity distribution, (b) Particle concentration distribution.

4. Further discussion

In a two-bed hospital ward heated by IJV, the influence of supply air parameters on exhaled particle dispersion were investigated in this study. T_s and ACH mainly affected the dispersion of fine particles with a diameter of ≤ 20 μm [59, 60]. The results showed that an increase in T_s promoted the removal of fine particles. It could be ascribed to that IJV delivered warm air downwards, increasing T_s could effectively elevate the air temperature at the floor level. After T_s increased, the upward movement of warm air became stronger [19, 61]. As a result, more fine particles could be carried into the upper zone of the ward and then removed through the ceiling outlet. Similar results were reported in radiant floor heating systems [55, 61]. Under the transient condition, Zhou et al. [61] compared the effect of the air temperature near floor on fine particle dispersion. The results showed that the increase in floor

temperature enhanced the effect of natural convection, resulting in accelerated particle removal.

The impact of *ACH* on particle dispersion was complex [62]. After the increase in *ACH* of IJV, the spreading distance of warm air was extended [33]. With appropriate supply air parameters, the warm airflow of IJV could comply with the direction of human body plume and exhalation flow, and exhibited a high performance in removing fine particles [39]. When *ACH* was excessive (more than 12 h^{-1}), indoor air mixing was enhanced. The removal fraction of fine particles became lower, while the suspension and deposition fractions increased, which might worsen air quality. Although the opinion of "the higher the *ACH*, the lower the exposure risk" was generally applied in practice to enhance the dilution of aerosols, the results from this study showed that an excessive *ACH* might reduce the removal of fine particles. The promotion of high *ACH* has been controversial [7]. Mousavi [63] found that a lower *ACH* could reduce turbulence and was helpful for contaminant containment. Mousavi and Grosskopf [64] quantified the effect of increasing *ACH* on the particle concentration. Their results showed that when an increase in *ACH* from 2.5 h^{-1} to 5.5 h^{-1}, the particle concentration at the breathing zone was more than 40% higher. Villafruela et al. [65] showed that an increase in *ACH* under DV system would increase the exposure risk in the isolation room. The similar findings could be found in non-hospital scenes [66]. Therefore, it was crucial to determine a suitable *ACH* in IJV heated ward. Using orthogonal-based grey relational method, this study recommended T_s of 28°C and *ACH* of 9 h^{-1} as the supply air parameters. The recommended supply air parameters can be used as a reference to guide the ventilation design in the ward heated by IJV.

5. Conclusions

To provide a healthy air environment for the occupants in hospital ward, this study proposed to apply IJV for hospital ward heating, with the hope of utilizing the high contaminant removal potential of IJV to reduce the cross-infection risk of occupants. Using CFD method, qualitative and quantitative effects of the supply air parameters of IJV on exhaled particle dispersion were revealed. Based on orthogonal design coupled with grey relational multi-objective optimization method, the supply air parameters were optimized. The main findings were as follows.

- The supply air parameters of IJV had important effects on particle dispersion in winter, with a total contribution percentage of 76.42% for $\eta_{removal}$ and 76.18% for τ, respectively.

- With the appropriate T_s and ACH, the warm airflow of IJV could comply with human body plume and enhance the removal of fine particles. However, at a low T_s (< 26°C) or an excessive ACH (> 12 h^{-1}), particle removal might be weakened.
- When $\eta_{removal}$ was used as the response indicator, the influencing factors in descending order were $ACH > T_s > T_{out} > IL$. When τ was used as the response indicator, the influencing factors in descending order were $ACH > T_{out} > T_s > IL$.
- Considering the effects of infector location and outdoor air temperature, the recommended supply air parameters of IJV for heating the hospital ward were ACH of 9 h^{-1} and T_s of 28°C.

Acknowledgement

This study was supported by National Natural Science Foundation of China (Grant No. 52378088) and Graduate Research and Innovation Foundation of Chongqing, China (Grant No. CYB23062).

References

[1] A. Ackley, O.I. Olanrewaju, O.N. Oyefusi, W.I. Enegbuma, T.S. Olaoye, A.E. Ehimatie, E. Ukpong, P. Akpan-Idiok, Indoor environmental quality (IEQ) in healthcare facilities: A systematic literature review and gap analysis. *Journal of Building Engineering*. 86 (2024) 108787. https://doi.org/10.1016/j.jobe.2024.108787

[2] R. Yam, P.L. Yuen, R. Yung, T. Choy, Rethinking hospital general ward ventilation design using computational fluid dynamics. *Journal of Hospital Infection*. 77(1) (2011) 31–36. https://doi.org/10.1016/j.jhin.2010.08.010

[3] S. Rayegan, C. Shu, J. Berquist, J. Jeon, L. Zhou, L.Z. Wang, H. Mbareche, P. Tardif, H. Ge, A review on indoor airborne transmission of COVID-19 – modelling and mitigation approaches. *Journal of Building Engineering*. 64 (2023) 105599. https://doi.org/10.1016/j.jobe.2022.105599

[4] H.T. Dao, K.S. Kim, Behavior of cough droplets emitted from COVID-19 patient in hospital isolation room with different ventilation configurations. *Building and Environment*. 209 (2022) 108649. https://doi.org/10.1016/j.buildenv.2021.108649

[5] T.J. Meerhoff, J.W. Paget, J.L. Kimpen, F. Schellevis, Variation of respiratory syncytial virus and the relation with meteorological factors in different winter seasons. *The Pediatric Infectious Disease Journal*. 28(10) (2009) 860–866. https://doi.org/10.1097/INF.0b013e3181a3e949

[6] A.D. Storms, M.D. Van Kerkhove, E. Azziz−Baumgartner, W.K. Lee, M.A. Widdowson, N.M.

Ferguson, A.W. Mounts, Worldwide transmission and seasonal variation of pandemic influenza A(H1N1) 2009 virus activity during the 2009–2010 pandemic. *Influenza and other respiratory viruses*. 7(6) (2013) 1328–1335. https://doi.org/10.1111/irv.12106

[7] T.W. Tsang, K.W. Mui, L.T. Wong, Computational Fluid Dynamics (CFD) studies on airborne transmission in hospitals: A review on the research approaches and the challenges. *Journal of Building Engineering*. 63 (2023) 105533. https://doi.org/10.1016/j.jobe.2022.105533

[8] M.K. Satheesan, K.W. Mui, L.T. Wong, A numerical study of ventilation strategies for infection risk mitigation in general inpatient wards. *Building Simulation*. 13 (2020) 887–896. https://doi.org/10.1007/s12273-020-0623-4

[9] S. Jo, G. Kim, M. Sung, A study on contaminant leakage from Airborne Infection Isolation room during medical staff entry; Implementation of walking motion on hypothetical human model in CFD simulation. *Journal of Building Engineering*. 86 (2024) 108812. https://doi.org/10.1016/j.jobe.2024.108812

[10] W. Su, Z.T. Ai, A. Melikov, Potential of a bed ventilation system in reducing the risk of exposure to contaminants in infectious wards. *Journal of Building Engineering*. 84 (2024) 108525. https://doi.org/10.1016/j.jobe.2024.108525

[11] M.P. Wan, C.Y.H. Chao, Y.D. Ng, G.N. Sze To, W.C. Yu, Dispersion of expiratory droplets in a general hospital ward with ceiling mixing type mechanical ventilation system. *Aerosol Science and Technology*. 41(3) (2007) 244–258. https://doi.org/10.1080/02786820601146985

[12] G.Y. Cao, I. Kvammen, T.A.S. Hatten, Y.X. Zhang, L. Stenstad, G. Kiss, J.G. Skogås, Experimental measurements of surgical microenvironments in two operating rooms with laminar airflow and mixing ventilation systems. *Energy and Built Environment*. 2(2) (2021) 149–156. https://doi.org/10.1016/j.enbenv.2020.08.003

[13] T. Li, E.A. Essah, Y.X. Wu, Y. Cheng, C.H. Liao, Numerical comparison of exhaled particle dispersion under different air distributions for winter heating. *Sustainable Cities and Society*. 89 (2023) 104342. https://doi.org/10.1016/j.scs.2022.104342

[14] P. Peng, C. Zhang, W.Q. Li, M. Pomianowski, G.C. Gong, X. Fang, L. Chun, R. Guo, Investigation on indoor airflow and contaminant dispersion of diffuse ceiling ventilation in heating and cooling modes. *Journal of Building Engineering*. 80 (2023) 107972. https://doi.org/10.1016/j.jobe.2023.107972

[15] S.L. Sinha, R.C. Arora, S. Roy, Numerical simulation of two-dimensional room air flow with and without buoyancy. *Energy and Buildings*. 32(1) (2000) 121–129. https://doi.org/10.1016/S0378-7788(99)00047-X

[16] B. Yang, A.K. Melikov, A. Kabanshi, C. Zhang, F.S. Bauman, G.Y. Cao, H.B. Awbi, H. Wigö, J.L. Niu, K.W.D. Cheong, K.W. Tham, M. Sandberg, P.V. Nielsen, R. Kosonen, R.M. Yao, S. Kato, S.C. Sekhar, S. Schiavon, T. Karimipanah, X.T. Li, Z. Lin, A review of advanced air distribution methods - theory, practice, limitations and solutions. *Energy and Buildings*. 202 (2019) 109359. https://doi.org/10.1016/j.enbuild.2019.109359

[17] Y.Z. Zhang, J.J. Liu, J.J. Pei, J.Y. Li, C.C. Wang, Performance evaluation of different air distribution systems in an aircraft cabin mockup. *Aerospace Science and Technology*. 70 (2017) 359–366. https://doi.org/10.1016/j.ast.2017.08.009

[18] H.J. Chen, B. Moshfegh, M. Cehlin, Computational investigation on the factors influencing thermal comfort for impinging jet ventilation. *Building and Environment*. 66 (2013) 29–41. https://doi.org/10.1016/j.buildenv.2013.04.018

[19] F.H. Cheng, S. Zhang, S.S. Gao, X. Tian, C.H. Liao, Y. Cheng, Experimental investigation of airflow pattern and turbulence characteristics of stratum ventilation in heating mode. *Building and Environment*. 186 (2020) 107339. https://doi.org/10.1016/j.buildenv.2020.107339

[20] T. Li, E.A. Essah, Y.X. Wu, C.H. Liao, Y. Cheng, Evaluation of heating performances of different ventilation methods in an office. *Indoor and Built Environment*. 33(3) (2024) 465–488. https://doi.org/10.1177/1420326X231200561

[21] Z. Lin, J.L. Wang, T. Yao, T.T. Chow, Investigation into anti-airborne infection performance of stratum ventilation. *Building and Environment*. 54 (2012) 29–38. https://doi.org/10.1016/j.buildenv.2012.01.017

[22] Y.F. Kang, H.G. Yin, J.L. Wang, D.N. Ji, J.Y. Zhang, X. Tian, Z.J. Ma, A.G. Li, Research on airflow convergence patterns and air distribution characteristics under multi-column attachment ventilation. *Building and Environment*. 245 (2023) 110862. https://doi.org/10.1016/j.buildenv.2023.110862

[23] H.G. Yin, L.N. Li, R. Wu, Y.Y. Wang, A.G. Li, A numerical study on the effect of column layout on air distribution and performance of column attachment ventilation. *Building Simulation*. 14 (2021) 1095–1108. https://doi.org/10.1007/s12273-020-0699-x

[24] H.G. Yin, Y.K. Huo, Y.Y. Wang, D.N. Ji, J.L. Wang, Z.J. Ma, A.G. Li, Numerical investigation on mechanisms and performance of column attachment ventilation for winter heating. *Building and Environment*. 202 (2021) 108025. https://doi.org/10.1016/j.buildenv.2021.108025

[25] Z. Lin, T.T. Chow, Y. Li, Deflection ventilation—A conceptual introduction. *Proceedings of 7th International Conference Healthy Buildings 2003*. Stallion Press, Singapore, pp. 363–369.

[26] F.H. Cheng, Y.H. Li, Y.X. Wu, Y. Cheng, Z. Lin, Experimental study of air distribution and heating

performances of deflection ventilation. *Energy and Buildings*. 282 (2023) 112800. https://doi.org/10.1016/j.enbuild.2023.112800

[27] T. Karimipanah, H.B. Awbi, Theoretical and experimental investigation of impinging jet ventilation and comparison with wall displacement ventilation. *Building and Environment*. 37 (2002) 1329–1342. https://doi.org/10.1016/S0360-1323(01)00117-2

[28] H.J. Chen, B. Moshfegh, M. Cehlin, Investigation on the flow and thermal behavior of impinging jet ventilation systems in an office with different heat loads. *Building and Environment*. 59 (2013) 127–144. https://doi.org/10.1016/j.buildenv.2012.08.014

[29] W. Su, B. Yang, A. Melikov, C.J.Y. Liang, Y.L. Lu f, F.M. Wang, A.G. Li, Z. Lin, X.T. Li, G.Y. Cao, R. Kosonen, Infection probability under different air distribution patterns. *Building and Environment*. 207 (2022) 108555. https://doi.org/10.1016/j.buildenv.2021.108555

[30] J. Hu, Y.M. Kang, J. Yu, K. Zhong, Numerical study on thermal stratification for impinging jet ventilation system in office buildings. *Building and Environment*. 196 (2021) 107798. https://doi.org/10.1016/j.buildenv.2021.107798

[31] C. Qin, Y.P. He, J. Li, W.Z. Lu, Mitigation of breathing contaminants: Exhaust location optimization for indoor space with impinging jet ventilation supply. *Journal of Building Engineering*. 69 (2023) 106250. https://doi.org/10.1016/j.jobe.2023.106250

[32] P. Rohdin, B. Moshfegh, Numerical predictions of indoor climate in large industrial premises. A comparison between different k–ε models supported by field measurements. *Building and Environment*. 42 (2007) 3872–3882. https://doi.org/10.1016/j.buildenv.2006.11.005

[33] X. Ye, Y.M. Kang, B. Zuo, K. Zhong, Study of factors affecting warm air spreading distance in impinging jet ventilation rooms using multiple regression analysis. *Building and Environment*. 120 (2017) 1–12. https://doi.org/10.1016/j.buildenv.2017.03.044

[34] A. Staveckis, A. Borodinecs, Impact of impinging jet ventilation on thermal comfort and indoor air quality in office buildings. *Energy and Buildings*. 235 (2021) 110738. https://doi.org/10.1016/j.enbuild.2021.110738

[35] H. Yamasawa, T. Kobayashi, T. Yamanaka, N. Choi, M. Cehlin, A. Ameen, Applicability of displacement ventilation and impinging jet ventilation system to heating operation. *Japan Architectural Review*. 4(2) (2021) 403–416. https://doi.org/10.1002/2475-8876.12220

[36] A. Ameen, M. Cehlin, U. Larsson, T. Karimipanah, Experimental investigation of ventilation performance of different air distribution systems in an office environment - Heating mode. *Energies*. 12 (2019) 1835. https://doi.org/10.3390/en12101835

[37] A. Ameen, M. Cehlin, H. Yamasawa, T. Kobayashi, T. Karimipanah, Energy saving, indoor

thermal comfort and indoor air quality evaluation of an office environment using corner impinging jet ventilation. *Developments in the Built Environment*. 15 (2023) 100179. https://doi.org/10.1016/j.dibe.2023.100179

[38] X. Ye, Y.M. Kang, F. Yang, K. Zhong, Comparison study of contaminant distribution and indoor air quality in large-height spaces between impinging jet and mixing ventilation systems in heating mode. *Building and Environment*. 160 (2019) 106159. https://doi.org/10.1016/j.buildenv.2019.106159

[39] L. Wang, X.H. Dai, J.J. Wei, Z.T. Ai, Y.F. Fan, L.L. Tang, T. Jin, J. Ge, Numerical comparison of the efficiency of mixing ventilation and impinging jet ventilation for exhaled particle removal in a model intensive care unit. *Building and Environment*. 200 (2021) 107955. https://doi.org/10.1016/j.buildenv.2021.107955

[40] L. Wang, Z.Q. Wang, S.R. Zhu, Z. Zhu, T. Jin, J.J. Wei, Numerical investigation of impinging jet ventilation in ICUs: Is thermal stratification a problem? *Building Simulation*. 16 (2023) 1173–1185. https://doi.org/10.1007/s12273-023-1023-3

[41] B. Zuo, K. Zhong, Y.M. Kang, An experimental study on particle resuspension in a room with impinging jet ventilation. *Building and Environment*. 89 (2015) 48–58. https://doi.org/10.1016/j.buildenv.2015.01.031

[42] C. Qin, W.Z. Lu, Effects of ceiling exhaust location on thermal comfort and age of air in room under impinging jet supply scheme. *Journal of Building Engineering*. 35 (2021) 101966. https://doi.org/10.1016/j.jobe.2022.105533

[43] A. Wang, L.L. Ding, M.L. Tan, S.J. Shi, B. Zhou, Numerical simulation on air distribution and aerosol transportation in operating room with unidirectional flow system under operational condition. *Journal of Building Engineering*. 80 (2023) 108004. https://doi.org/10.1016/j.jobe.2023.108004

[44] I. Olmedo, F.A. Berlanga, J.M. Villafruela, M. Ruiz de Adana, Experimental variation of the personal exposure in a hospital room influenced by wall heat gains. *Building and Environment*. 154 (2019) 252–262. https://doi.org/10.1016/j.buildenv.2019.03.008

[45] GB 50189-2015, *Design standard for energy efficiency of public buildings*. Ministry of Housing and Urban-Rural Development of the People's Republic of China, Beijing, China, 2015.

[46] D.Y. Tan, B.Z. Li, Y. Cheng, H. Liu, J.H. Chen, Airflow pattern and performance of wall confluent jets ventilation for heating in a typical office space. *Indoor and Built Environment*. 29(1) (2020) 67–83. https://doi.org/10.1177/1420326X19842632

[47] Z.J. Liu, T.C. Wang, Y.X. Wang, H.Y. Liu, G.Q. Cao, S. Tang, The influence of air supply inlet

location on the spatial-temporal distribution of bioaerosol in isolation ward under three mixed ventilation modes. *Energy and Built Environment*. 4(4) (2022) 445–457. https://doi.org/10.1016/j.enbenv.2022.03.002

[48] C. Chen, B. Zhao, Some questions on dispersion of human exhaled droplets in ventilation room: answers from numerical investigation. *Indoor Air*. 20 (2010) 95–111. https://doi.org/10.1111/j.1600-0668.2009.00626.x

[49] B. Zhao, Y. Zhang, X.T. Li, X.D. Yang, D.T. Huang, Comparison of indoor aerosol particle concentration and deposition in different ventilated rooms by numerical method. *Building and Environment*. 39 (2004) 1–8. https://doi.org/10.1016/j.buildenv.2003.08.002

[50] C.K. Lai Alvin, F.Z. Chen, Modeling particle deposition and distribution in a chamber with a two-equation Reynolds-averaged Navier–Stokes model. *Aerosol Science*. 37(12) (2006) 1770–1780. https://doi.org/10.1016/j.jaerosci.2006.06.008

[51] X. Ye, H. Zhu, Y.M. Kang, K. Zhong, Heating energy consumption of impinging jet ventilation and mixing ventilation in large-height spaces: A comparison study. *Energy and Buildings*. 130 (2016) 697–708. https://doi.org/10.1016/j.enbuild.2016.08.055

[52] F.Z. Chen, S.C.M. Yu, A.C.K. Lai, Modeling particle distribution and deposition in indoor environments with a new drift–flux model. *Atmospheric Environment*. 40 (2006) 357–367. https://doi.org/10.1016/j.atmosenv.2005.09.044

[53] J.M. Villafruela, I. Olmedo, J.F. San Jose, Influence of human breathing modes on airborne cross infection risk. *Building and Environment*. 106 (2016) 340–351. https://doi.org/10.1016/j.buildenv.2016.07.005

[54] Q. Zhou, H. Qian, H.G. Ren, Y.G. Li, P.V. Nielsen, The lock-up phenomenon of exhaled flow in a stable thermally-stratified indoor environment. *Building and Environment*. 116 (2017) 246–256. https://doi.org/10.1016/j.buildenv.2017.02.010

[55] A. Jurelionis, L. Stasiuliene, T. Prasauskas, D. Martuzevicius, Dispersion of indoor air pollutants emitted at near-floor levels in rooms with floor heating and mixing ventilation. *Indoor and Built Environment*. 27(2) (2018) 205–218. https://doi.org/10.1177/1420326X16669975

[56] A. Agirman, Y.E. Cetin, M. Avci, O. Aydin, Effect of air exhaust location on surgical site particle distribution in an operating room. *Building Simulation*. 13 (2020) 979–988. https://doi.org/10.1007/s12273-020-0642-1

[57] C.F. Jeffrey Kuo, T.L. Su, P.R. Jhang, C.Y. Huang, C.H. Chiu, Using the Taguchi method and grey relational analysis to optimize the flat-plate collector process with multiple quality characteristics in solar energy collector manufacturing. *Energy*. 36(5) (2011) 3554–3562.

https://doi.org/10.1016/j.energy.2011.03.065

[58] Y. Kuo, T. Yang, G.W. Huang, The use of grey relational analysis in solving multiple attribute decision-making problems. *Computers and Industrial Engineering*. 55(1) (2008) 80–93. https://doi.org/10.1016/j.cie.2007.12.002

[59] H. Qian, Y.G. Li, Removal of exhaled particles by ventilation and deposition in a multibed airborne infection isolation room. *Indoor Air*. 20 (2010) 284–297. https://doi.org/10.1111/j.1600-0668.2010.00653.x

[60] M. Abuhegazy, K. Talaat, O. Anderoglu, S.V. Poroseva, Numerical investigation of aerosol transport in a classroom with relevance to COVID-19. *Physics of Fluids*. 32 (2020) 103311. https://doi.org/10.1063/5.0029118

[61] Y. Zhou, Y.L. Deng, P. Wu, S.J. Cao, The effects of ventilation and floor heating systems on the dispersion and deposition of fine particles in an enclosed environment. *Building and Environment*. 125 (2017) 192–205. https://doi.org/10.1016/j.buildenv.2017.08.049

[62] M. Sandberg, The dual role of an air distribution system, both reducing the concentration of infectious agents and spreading infectious agents. *Frontiers in Built Environment*. 7 (2022) 728968. https://doi.org/10.3389/fbuil.2021.728968

[63] E.S. Mousavi, Toward an energy efficient healthcare environment: a case study of hospital corridor design. *International Journal of Environmental Science and Technology*. 16 (2019) 7633–7642. https://doi.org/10.1007/s13762-019-02386-4

[64] E.S. Mousavi, K.R. Grosskopf, Ventilation rates and airflow pathways in patient rooms: a case study of bioaerosol containment and removal. *Annals of Occupational Hygiene*. 59(9) (2015) 1190–1199. https://doi.org/10.1093/annhyg/mev048

[65] J.M. Villafruela, I. Olmedo, F.A. Berlanga, M. Ruiz de Adana, Assessment of displacement ventilation systems in airborne infection risk in hospital rooms. *Plos One*. 14(1) (2019) e0211390. https://doi.org/10.1371/journal.pone.0211390

[66] J. Pantelic, K.W. Tham, Adequacy of air change rate as the sole indicator of an air distribution system's effectiveness to mitigate airborne infectious disease transmission caused by a cough release in the room with overhead mixing ventilation: A case study. *HVAC and R Research*. 19(8) (2013) 947–961. https://doi.org/10.1080/10789669.2013.842447